Power generation from commercial turbochargers connected in parallel

Van der Merwe A.H
Supervisor: Le Roux W.G.
Department of Mechanical and Aeronautical Engineering, University of Pretoria,
Private Bag X20, Hatfield, Pretoria 0028, South Africa
U17023735@gmail.com

Centre for Renewable and Sustainable Energy Studies

Abstract
Countries such as South Africa are struggling to supply enough power to its citizens due to a failing power grid. This creates an opportunity for the development of small-scale power generation. This study investigates a parallel flow micro-turbine using off-the-shelf Garrett turbochargers for power generation. Two different configurations are modelled, namely, a low-temperature turbine (LTT) and a high-temperature turbine (HTT) where the only difference is the position of the power turbine. In this initial study, both configurations are modelled at steady state for unrecuperated cycles without pressure losses. It was found that the HTT is superior to the LTT configuration when no pressure losses are introduced. Results show that the GT2860RS turbocharger as gasifier combined with the GT1241 as power turbine produces the highest efficiency at the highest pressure ratio. Overall, the results show that an unrecuperated HTT can generate between 1.5 kW and 7.2 kW of power with a thermal efficiency of up to 6%.

Keywords: Brayton cycle, micro-turbine, parallel, turbocharger, turbo-generator.

1. Introduction
Globally there are about 1.1 billion people who do not have access to a national grid of which 84% are living in rural and remote areas in developing countries (De Almeida et al., 2020). The lack of power supply presents the opportunity for small-scale power generation (Ouedraogo, 2019). Personal micro-turbine power generation systems may in future become as normal as owning a personal computer (McDonald and Rodgers, 2002). A recuperator is usually added to transfer waste heat to the cold compressed air to improve the cycle efficiency by decreasing the amount of heat needed to reach a specific combustion outlet temperature (Xiao et al., 2017; Dellar et al., 2020). The remaining exhaust heat can be applied for water heating (Le Roux, 2018; Visser et al., 2011), absorption chilling or desalination (Gomri, 2010). Furthermore, micro-turbines can utilise a wide range of fuels including hydrogen (McDonald and Rodgers, 2002) and concentrated solar power (Le Roux and Sciacovelli, 2019). Thermal storage methods such as packed rock bed (Allen, 2010) and solar salts (Humbert et al., 2022) have also been proposed for micro-turbines.

A turbocharger can be applied to construct a micro-turbine cycle (Brayton power cycle) because it already consists of a turbine and compressor wheel fixed on a common shaft (Ibaraki et al., 2006). Turbochargers are readily available and thus affordable (Visser et al., 2011), and have been developed for many decades to perform well at the proposed operating conditions of up to 950 °C (Shah, 2005) and 1050°C intermittently (Le Roux and Sciacovelli, 2019). Off-the-shelf turbochargers have also been proposed to act as micro-turbines in solar-dish Brayton cycles, in order to reduce overall cycle costs (Mills, 2004) with high reliability (Pietsch and Brandes, 1989). Le Roux and Sciacovelli (2019) performed an analysis on an open-cavity tubular solar receiver with integrated metallic phase-change material (PCM) for short-term thermal storage, together with an off-the-shelf turbocharger for power generation in a recuperated solar-dish Brayton cycle. They showed that maximum solar-to-mechanical efficiencies of 10% to 15% could be achieved at receiver temperatures of between 900 K and 1200 K.

In recent years, many studies have been done on combining an off-the-shelf turbocharger with a generator for different applications. Companies like MTT (MTT, 2022) have developed a 3 kW recuperated micro-turbine generator from off-the-shelf turbochargers to present a more cost-effective product (Visser et al., 2011). The automobile industry uses electrically assisted turbochargers to increase turbo response (Subramaniam and Salim, 2021; Hong et al., 2018). Noguchi et al. (2007) used an ultrahigh-speed permanent magnet synchronous motor drive connected to an automobile's turbocharger to produce 2.2 kW at 120 000 rpm using the combustion energy from exhaust gas. Lee and Hong (2021) developed a high-speed surface-mounted permanent magnet synchronous motor that produced 3 kW while operating at 100 000 rpm to review the effect of eccentricity that affects the vibrations. Lim et al. (2017) also investigated speed response characteristics of an electrically assisted turbocharger that produced 4 kW at 150 000 rpm.

Besides using an electrically assisted turbocharger to improve performance, turbochargers have also been adapted to be used as micro-turbine range extenders. Delta Cosworth developed a recuperated micro-turbine range extender (MiTRE) for significant weight advantages and simple integration with an electric vehicle (Delta-Cosworth, 2021). Compared to other micro-turbines, MiTRE is inexpensive with low maintenance due to the single moving part (Delta-Cosworth, 2021). Metis Design Corporation (MDC) developed a unique two-spool micro gas turbine (MGT) with a precombustion low-temperature power turbine connected in series with the gasifier. The power output of this MGT was 40 kW with a recuperator efficiency of 60% and an electrical efficiency of 21% (Keogh, 2015).

When considering the literature on micro-turbines, the generator is usually connected directly to the main shaft (single-shaft) or the power turbine with the generator is connected in series with the gasifier (twin-shaft) as shown in Ssebabi et al. (2019). The novelty of the current work is the investigation of a power turbine connected in parallel with the gasifier. Off-the-shelf Garrett turbochargers are considered for both the power turbine and the gasifier. Furthermore, two different concepts are modelled where the only difference is the position of the parallel-connected power turbine. The first concept is a low-temperature turbine (LTT) connected in parallel before the combustor and the second concept is a high-temperature turbine (HTT) connected in parallel after the combustor.

2. Research methodology

When using a turbocharger as a microturbine, a few difficulties have to be overcome when considering the method of connecting a generator to the turbine. These difficulties include running at high speeds and operating at high temperatures. The feasibility of a low-temperature turbine will be weighed up against a high-temperature turbine configuration. The low-temperature turbine eliminates the challenges faced with high temperature connections, making it easier to connect to a gearbox or generator. Therefore, a low-temperature concept is favoured. The theoretical analysis and the layouts of these concepts are to be discussed in the following sections.

2.1. LTT and HTT concepts

The layout of the LTT concept is shown in Figure 1. The selected Garrett turbochargers use oil or water as coolant to prevent it from overheating (Garrett, 2020). The combustor is to be connected to the turbocharger between the compressor and the gas turbine to complete the Brayton cycle. The gasifier does not have any external loads connected to the shaft. A generator is simulated in the model simply by calculating the available power output from the secondary low-temperature turbine called the power turbine. The power turbine consumes a fraction of the compressed air flowing from the compressor.

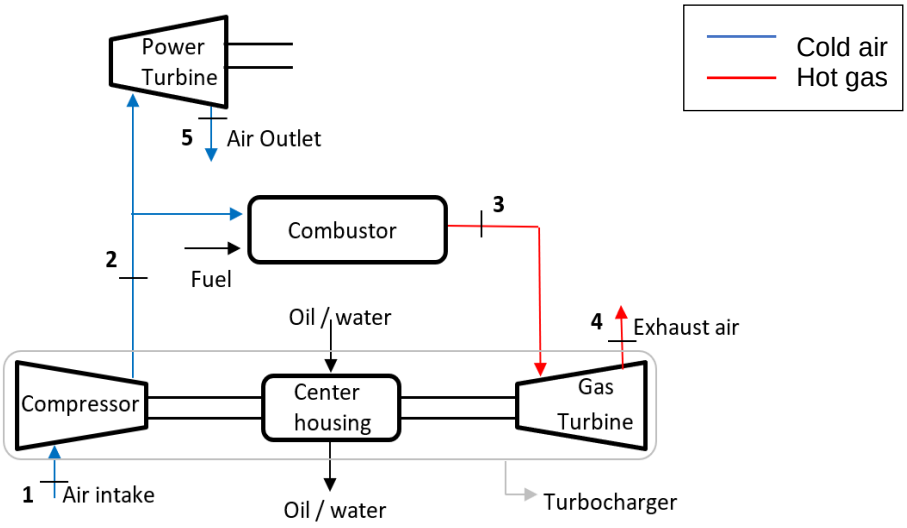

Figure 1: Parallel-integrated, low-temperature turbine.

The high-temperature turbine concept, shown in Figure 2, will be connected directly after the combustor in parallel and consuming a fraction of the combustion gas flow.

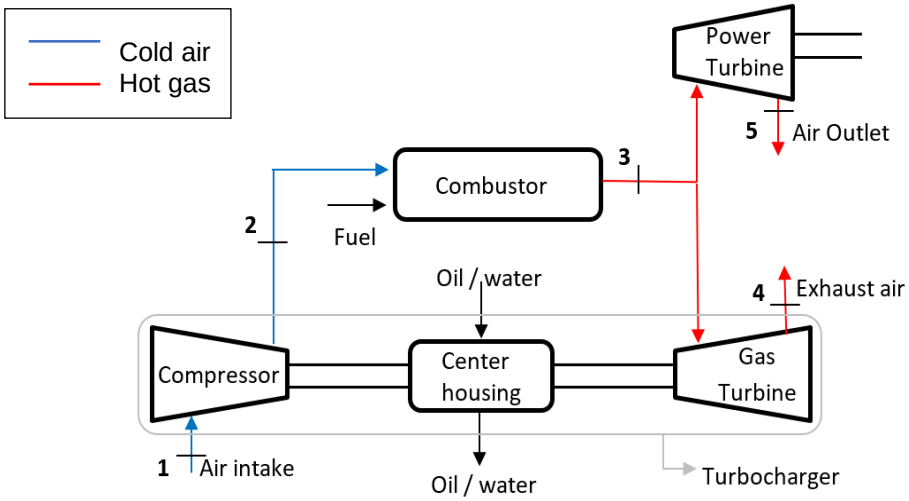

Figure 2: Parallel-integrated, high-temperature turbine.

2.2. Modelling procedure

The compressor and turbine maps for the Garrett turbocharger were available from Garrett (2020). An image digitiser ("WebPlotDigitizer", which uses Java programming) was used to generate functional data in coordinate format from the map images. B-spline modelling from the built-in scipy.interpolate function in Python was used to fit a line through all of the coordinates. This model allowed for the data sets to be imported into Python. The datasets were personalized for finding revolutions per minute (RPM) and isentropic efficiency for each operating point on the compressor and turbine maps. The corrected mass flow rates of the compressor map and the turbine map were also converted from lbs/min to kg/s. The data was then imported and applied for simulations by iterating through a range of pressure ratios in each data set, starting from 1.4 and ending when the edge of a compressor map was reached for either the gas turbine or the power turbine. A Python programming solution solved for the RPM and isentropic efficiency given the pressure ratio and the compressor corrected mass flow rate in coordinate format. The theoretical model's objective was to find the power produced by the power turbine as well as the cycle's thermal efficiency.

2.3. Low-temperature turbine (LTT) analysis

To determine the power output, the mass flow rate and the change in temperature over the turbine are required. The properties in the power turbine section can be approximated to be the same as the outlet properties of the compressor, assuming no heat and pressure losses in the piping section. To determine the outlet temperature of the compressor, the power consumed by the compressor is needed. For a turbocharger, the power consumed by the compressor is assumed to be equal to the power produced by the gas turbine, since they are connected on the same shaft. To determine the gas turbine's power output, the compressor corrected flow and power turbine's corrected flow is required in order to determine the RPM value which is needed for the blade speed ratio (BSR) to calculate the gas turbine's efficiency. A high-level iteration scheme was therefore required because the compressor and gas turbine were dependent on each other. It is for this reason that it was decided to start from the two turbine outlets using their respective maps to solve the unknowns simultaneously. It is assumed that the components are well insulated. The assumed inputs for the system are as follows: $P_1 = P_{atm} = 87\ kPa$, $T_1 = T_{ambient} = 300K$, $r_c = r_{GT} = r_{PT}$, $P_2 = P_3$, $k_{air} = 1.4$ and $k_g = 1.333$. For the first iteration, the compressor's pressure and isentropic temperature at the outlet can be calculated from Equations 1 and 2, respectively.

$$P_2 = P_1 * r_c \tag{1}$$

$$T_{2,s} = T_1 * r_c^{\left(\frac{k_{air}-1}{k_{air}}\right)} \tag{2}$$

Secondly, the corrected mass flow rates for the two turbines can be read off from the turbine maps after T_2 and T_3 are assumed. The turbine corrected mass flow rates, in kg/s, can be converted to actual mass flow rates using Equations 3a and 3b based on the turbine inlet temperatures in Kelvin and the inlet pressures in Pascal (Le Roux and Sciacovelli, 2019).

$$\dot{m}_{PT,AF} = \dot{m}_{PT,CF} \frac{\left(\frac{P_2}{14.7 * 6894.8}\right)}{\sqrt{\frac{\left((T_2 - 273.15) * 1.8 + 492\right)}{519}}} \tag{3a}$$

$$\dot{m}_{GT,AF} = \dot{m}_{GT,CF} \frac{\left(\frac{P_3}{14.7 * 6894.8}\right)}{\sqrt{\frac{\left((T_3 - 273.15) * 1.8 + 492\right)}{519}}} \tag{3b}$$

The total compressor corrected mass flow rate can now be calculated by adding the two actual turbine mass flow rates (refer to Equation 4) and substituting the result into Equation 5. Note that the temperature is in Kelvin, and the pressure is in Pascal (Le Roux and Sciacovelli, 2019).

$$\dot{m}_{TOT} = \dot{m}_{GT,AF} + \dot{m}_{PT,AF} \tag{4}$$

$$\dot{m}_{c,CF} = \dot{m}_{TOT} \cdot \frac{\sqrt{\frac{(T_1 - 273.15) * 1.8 + 492}{545}}}{\left(\frac{P_1}{13.95 * 6894.8}\right)} \tag{5}$$

To find the correct power turbine inlet temperature, the compressor power which is equal to the available gas turbine power is needed. Since an initial value for the compressor corrected flow rate has been calculated, the available power produced by the gas turbine can be approximated after finding the BSR and the turbine isentropic efficiency using Equations 6 and 7, respectively (Le Roux and Sciacovelli, 2019).

For the BSR, the enthalpy at the turbine's inlet and the turbine's RPM is to be found. The required enthalpy at the inlet of the turbine is computed via interpolation using the CoolProp library in Python, similar to the ideal gas property tables in Borgnakke & Sonntag (2017), after assuming the turbine inlet temperature.

$$BSR = \frac{\left({}^{2\pi N}/_{60}\right) * \left({}^{d_t}/_{2}\right)}{\sqrt{2 * h_3\left(1 - \left(r_{GT}\right)^{\frac{1-k_g}{k_g}}\right)}} \tag{6}$$

$$\eta_t = \eta_{t,max} * \left[1 - \left(\frac{BSR - 0.6}{0.6}\right)^2\right] \tag{7}$$

The turbine's exducer diameter for Equation 6 is available from Garrett (2020). The only remaining variable for calculating the available gas turbine power using Equation 9 is the isentropic outlet temperature, calculated with Equation 8.

$$T_{4,s} = T_3 * \left(\frac{1}{r_{GT}}\right)^{\frac{k_g-1}{k_g}} \tag{8}$$

$$\dot{W}_{GT} = \eta_t \dot{\mathrm{m}}_{GT,AF} C_{pg} \left(T_3 - T_{4,s}\right) \tag{9}$$

Note that the isentropic outlet temperature of the gasifier's turbine is calculated with Equation 8, whereas the low-temperature power turbine is dependent on the compressor outlet temperature as shown in Equation 10 below.

$$T_{5,s} = T_2 * \left(\frac{1}{r_{PT}}\right)^{\frac{k_{air}-1}{k_{air}}} \tag{10}$$

The outlet temperature of the gasifier's turbine is found using Equation 11 when assuming a constant C_{pg} value based on the average temperature over the turbine.

$$T_4 = T_3 - \left(\frac{\dot{W}_{GT}}{\dot{\mathrm{m}}_{GT,AF} * C_{pg}}\right) \tag{11}$$

To calculate the power turbine's power output using Equation 12, the following is needed: the isentropic outlet temperature using Equation 10, the temperature at the compressor outlet, the RPM of the power turbine shaft (found from its virtually-connected compressor map), the power turbine's efficiency using Equation 7 and the constant C_p value based on the average temperature over the turbine. Finally, the combustion chamber heat input is computed with Equation 13 to solve the cycle's thermal efficiency with Equation 14 below.

$$\dot{W}_{PT} = \eta_t * \dot{\mathrm{m}}_{PT,AF} * C_{pg} * \left(T_2 - T_{5,s}\right) \tag{12}$$

$$\dot{Q}_{in} = \dot{m}_{GT,AF} * C_{pg} * \left(T_4 - T_3\right) \tag{13}$$

$$\eta_{cycle} = \frac{\dot{W}_{PT}}{\dot{Q}_{in}} \tag{14}$$

The iterative model, using the *scipy.optimize.minimise* library in Python, will optimise the temperatures T_2 and T_3 so that the gas turbine's power calculated with Equation 9 is equal to the compressor power calculated with Equation 15, while also adhering to the 1st law shown in Equation 16.

$$\dot{W}_c = \frac{\dot{W}_{c,s}}{\eta_c} = \frac{\dot{m}_{TOT} * C_{p,s} * (T_{2,s} - T_1)}{\eta_c} \quad (15)$$

$$\dot{W}_{PT} + \dot{m}_{GT,AF} * h_4 + \dot{m}_{PT,AF} * h_5 = \dot{Q}_{in} + \dot{m}_{TOT} * h_1 \quad (16)$$

A summary of the iteration process is visually represented in Figure 3. The iteration process starts by selecting a pressure ratio, getting the turbine mass flow rates and calculating the compressor corrected flow using Equation 5.

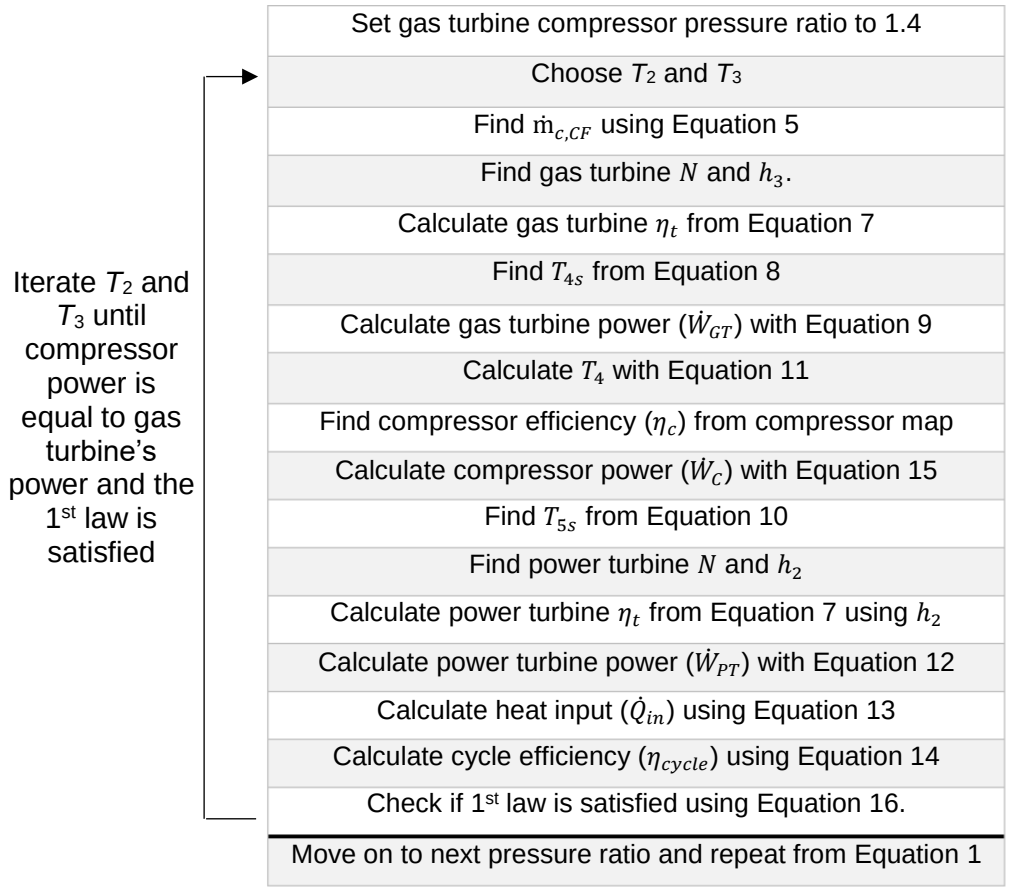

Figure 3: Representation of the LTT iterative process used in the model.

2.4. High-temperature turbine (HTT) analysis

The theoretical analysis for the HTT is not much different from the LTT analysis. Please refer to Figure 2 for the system layout. The power turbine inlet temperature changes throughout the model from T_2 to T_3, the mass flow rate through the combustion chamber is changed to the total air flow supplied by the compressor as shown in Equation 20 and lastly, the *k*-value used in Equation 10 is changed to the gas *k*-value as used for the gas turbine (see Equation 17). Hence, the steps discussed for the LTT are followed with minor differences. The first alteration in the model is to use the combustion chamber outlet properties whenever calculating the actual mass flow rate according to Equation 18. The second alteration is to calculate the power output of the power turbine with the combustion outlet temperature as the turbine inlet temperature using Equation 19.

$$T_{5,s} = T_3 * \left(\frac{1}{r_{PT}}\right)^{\frac{k_{air}-1}{k_{air}}} \quad (17)$$

$$\dot{m}_{PT,AF} = \dot{m}_{PT,CF} \frac{\left(\frac{P_3}{14.7 * 6894.8}\right)}{\sqrt{\frac{\left((T_3 - 273.15) * 1.8 + 492\right)}{519}}} \quad (18)$$

$$\dot{W}_{PT} = \eta_t * \dot{m}_{PT,AF} * C_{pg} * \left(T_3 - T_{5,s}\right) \quad (19)$$

$$\dot{Q}_{in} = \dot{m}_{TOT} * C_{pg} * (T_4 - T_3) \quad (20)$$

Similar to the iteration diagram above, Figure 4 shows the steps taken to model the HTT configuration.

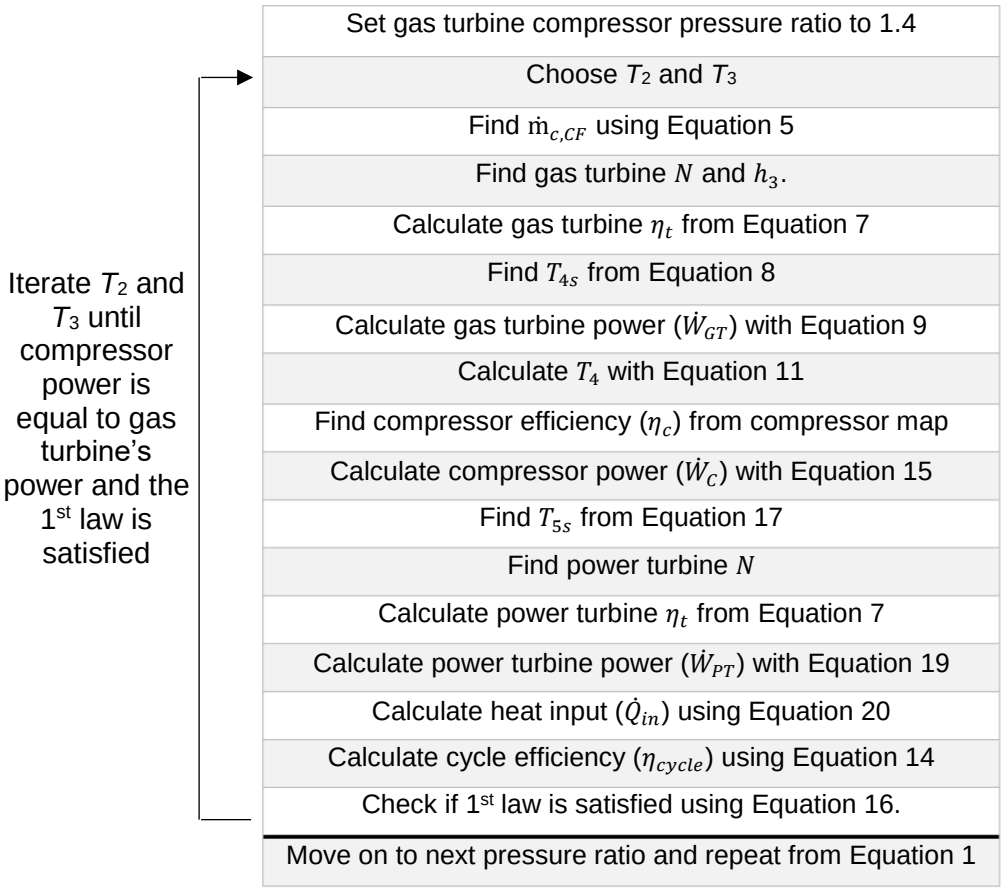

Figure 4: Representation of the HTT iterative process used in the model.

2.5. Cogeneration

As mentioned in Chapter 1, the exhaust heat can be used in different applications to increase the energy utilization factor (EUF). In this paper, the EUF is used as an extra validation to the model to see if the power generation plus the rate of heat transferred to the surroundings is equal to the total rate of heat input into the system. Equation 14 is modified to include the exhaust heat from both turbines to calculate the EUF with Equation 21.

$$EUF = \frac{\dot{W}_{PT} + \dot{m}_{GT} * (h_4 - h_1) + \dot{m}_{PT} * (h_5 - h_1)}{\dot{Q}_{in}} \quad (21)$$

3. Results

The complete GT2860RS turbocharger is used as the gasifier whereas only the turbine of the GT1241 is used as the power turbine. Even though only the turbocharger's turbine is required for the power turbine (to be connected to a generator directly or via a gearbox) in a physical setup, this turbocharger's compressor map is still implemented to determine the turbine's RPM for the theoretical model (since speed lines are not included in Garrett's turbine maps). For the model to be able to run, the compressor should be sized large enough to supply enough mass flow rate to both turbines without choking and when choosing a turbocharger with a large compressor, its corresponding turbine is also large. This results in the power turbine to be smaller than the gasifier.

3.1. Low-temperature turbine (LTT) results

The results for the low-temperature power turbine (LTT) without any pressure losses are shown in Figure 5 for the power output and thermal efficiency respectively. The operating range of the gas turbine and the power turbine is each plotted on their respective compressor maps in Figure 6 to get a visual representation of how efficient the turbochargers are running. The compressor outlet temperature is also added to get an idea what the temperatures are before combustion.

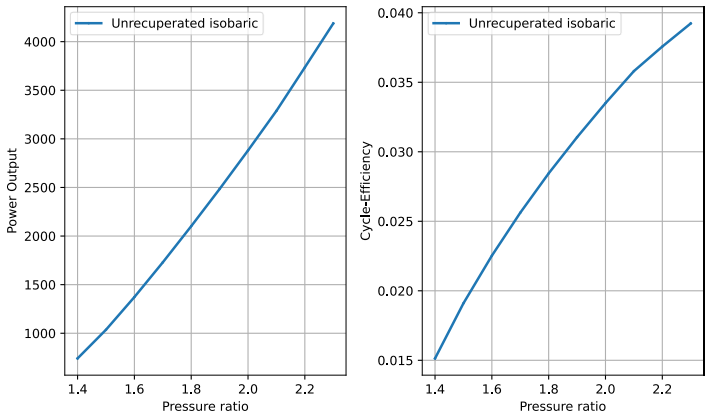

Figure 5: Power output [W] and thermal efficiency for the LTT configuration.

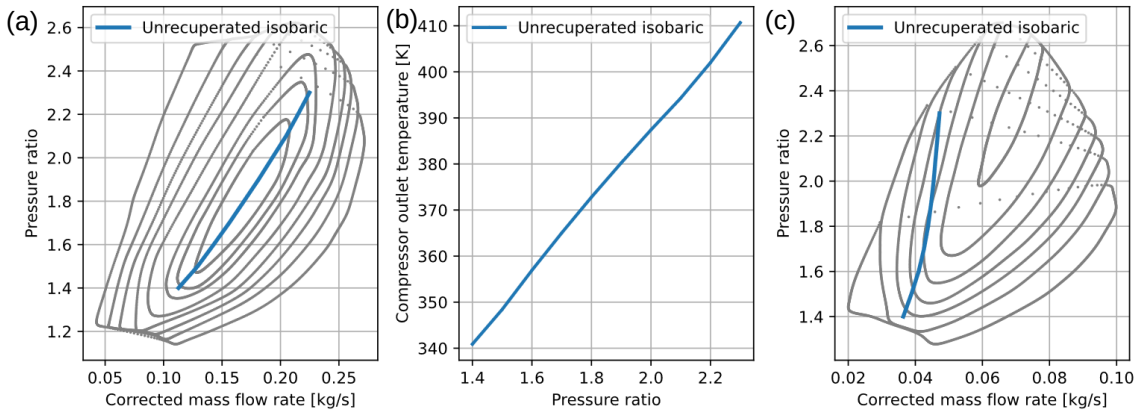

Figure 6: LTT (a) operating range of the gas turbine and (b) compressor outlet temperature for the GT2860RS gasifier with (c) operating range of the GT1241 as power turbine on virtual compressor map (using compressor maps digitised from Garrett, 2020).

The EUF for the LTT, in Figure 7, validated that all of the energy added to the system was either used to produce useful power output or was expelled to the atmosphere (assuming

100% efficient heat exchangers – for example, to heat water in cogeneration) because the EUF is equal to 1 regardless of the operating point.

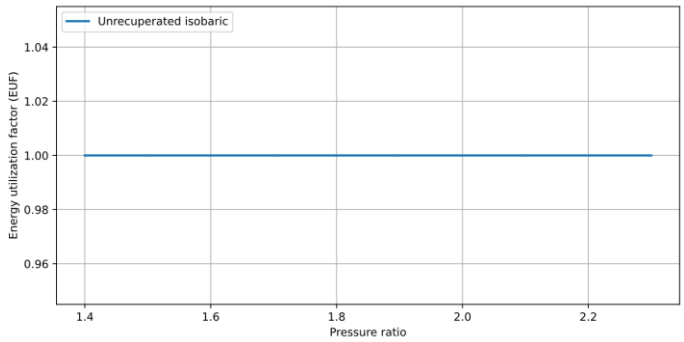

Figure 7: EUF for the LTT when all the exhaust gases are utilised.

3.2. High-temperature turbine (HTT) results

The same analysis was followed for the HTT configuration. The results for the high-temperature power turbine (HTT) are shown in Figure 8 for the power output and thermal efficiency respectively. The operating range of the gasifier's turbine, the outlet temperature of the compressor and the operating range of the power turbine (visualised using the virtual compressor map) is shown in Figure 9.

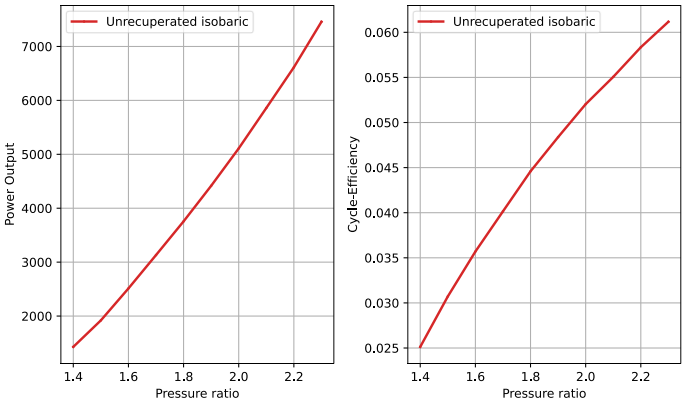

Figure 8: Power output [W] and thermal efficiency for the HTT configuration.

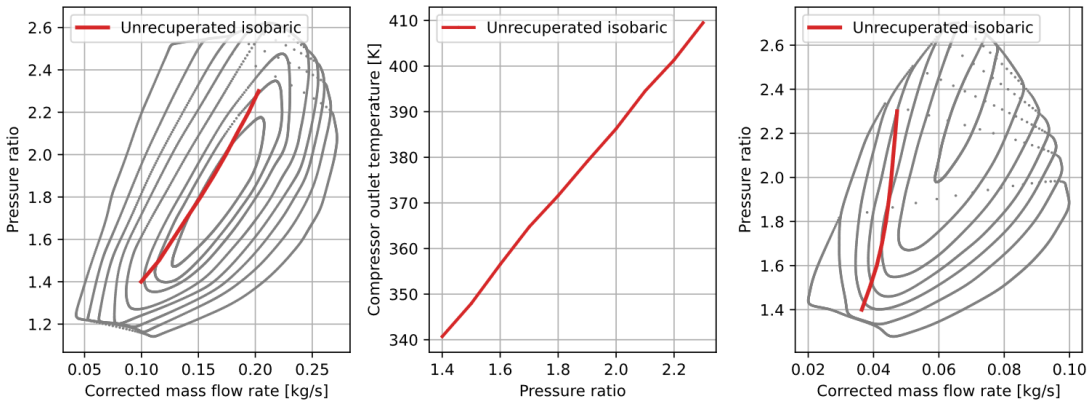

Figure 9: HTT (a) operating range of the gas turbine and (b) compressor outlet temperature for the GT2860RS gasifier with (c) operating range of the GT1241 as power turbine on virtual compressor map (using compressor maps digitised from Garrett, 2020)

The EUF for the HTT, in Figure 10, again validated that all of the energy added to the HTT system was either used to produce useful power output or was expelled to the atmosphere because it is equalled 1 regardless of the operating point.

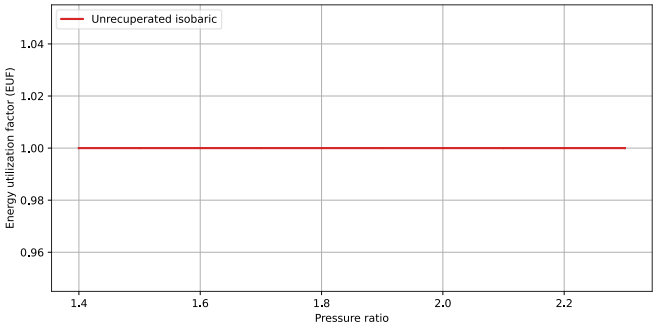

Figure 10: EUF for the HTT when all the exhaust gases are utilised.

Figure 9 shows that there is potential for higher power output at higher pressure ratios, however, the power turbine cannot be simulated any further due to surging on the virtual compressor map.

4. Conclusions and recommendations

4.1. Summary

In this paper, the authors investigated a small-scale parallel-flow turbo-generator by modelling two different variations of the proposed micro-turbine. These variations included a low-temperature and high-temperature parallel-flow turbine for power generation. The parallel flow configuration functions by maintaining system operation via the gasifier while the power turbine is used to generate power using only a fraction of the air coming out of the compressor. Off-the-shelf Garrett turbochargers were modelled for both the high-temperature and low-temperature concepts. It is expected that the operating cost and maintenance cost will be less when using an off-the shelf turbocharger as a micro-turbine.

4.2. Conclusion

The analysis found that the unrecuperated high-temperature turbine produced more power and had a higher thermal efficiency than the low-temperature turbine. The maximum power output and cycle efficiency for the LTT was found to be 4.2 kW and 3.9 %, respectively at a pressure ratio of 2.3. The HTT, for the same combination, yielded a maximum power output and cycle efficiency of 7.2 kW and 6 % at a pressure ratio of 2.3. From Figure 9a it can be noted that the HTT is operating at a lower corrected mass flow rate compared to the LTT in Figure 6a. This means that, for the HTT, a larger power turbine could be used which requires a larger mass flow rate without the compressor choking, but this is not necessarily true for the LTT.

In conclusion, an unrecuperated LTT turbine without any pressure losses is less efficient and produces less power compared to the HTT configuration, which results in the HTT being the best solution in this initial conceptual study. However, the lower temperatures of the LTT present a lower risk and longer lifespan to the power turbine.

4.3. Future work and recommendations

Future work will include adding a recuperator to the model to increase the efficiency for both configurations and also to see what effect pressure losses will have. Furthermore, it is recommended that a cost analysis be done on the operating costs and maintenance costs of the proposed turbo-generator. Lastly, the effect of all heat losses included that were assumed to be negligible in this study should also be investigated.

Nomenclature

Symbols

C_p	Air isobaric specific heat [J/kgK]
C_{pg}	Gas isobaric specific heat [J/kgK]
d_t	Turbine exducer diameter [mm]
h	Enthalpy [J/kg]
k	Ratio of specific heat
$\dot{m}$	Mass flow rate [kg/s]
N	Rotational speed [RPM]
P	Pressure [Pa]
Q	Heat input [W]
$\dot{Q}$	Heat transfer rate [W]
r	Pressure ratio
T	Temperature [K]
T_s	Isentropic temperature [K]
$\dot{W}$	Power output [W]

Greek symbols

η	Thermal efficiency

Subscripts

1-5	At state 1-5
AF	Actual flow
air	Of the air
CF	Corrected flow
fuel	Of the fuel
GT	Of the gas turbine
PT	Power turbine
TOT	Total

Abbreviations

BSR	Blade speed ratio
MGT	Micro gas turbine
RPM	Revolutions per minute

References

Allen, K.G. (2010) Performance characteristics of packed bed thermal energy storage for solar thermal power plants, Thesis: University of Stellenbosch.

Borgnakke, C., & Sonntag, R. E. (2017). Fundamentals of Thermodynamics 7th Edition SI version. Singapore: John Wiley & Sons.

Çengel, Y. A., & Ghajar, A. J. (2015). Heat and Mass Transfer: Fundamentals & Applications, Fifth Edition in SI Units, New York, McGraw-Hill.

De Almeida, A., Moura, P., Quaresma, N. (2020) "Energy-efficient off-grid systems—review," *Energy Efficiency*, 13(2), pp. 349–376. doi:10.1007/s12053-019-09813-y.

DELLAR KE, LE ROUX WG and MEYER JP (2020) Plate-style recuperator for a solar Brayton cycle using high-temperature sealant, Applied Thermal Engineering 177: 115439.

Delta-Cosworth. (2021) *Catalytic Generator - Zero Emissions Capable*. [online] Available

at: <https://www.cosworth.com/capabilities/electrification/hybrid-solutions/catalytic-generator/>.

Garrett. (2020) Performance Turbochargers - Garrett - G GT GTX GTW Series Turbo TBG. [online] Available at: <https://www.garrettmotion.com/racing-and-performance/performance-turbos/> [Accessed 28 August 2020].

Gomri, R. (2010) Thermal seawater desalination: Possibilities of using single effect and double effect absorption heat transformer systems. *Desalination*, 253(1-3), pp.112-118.

Hong, D., Lee, T. and Jeong, Y., (2018) "Design and Experimental Validation of a High-Speed Electric Turbocharger Motor Considering Variation of the L/D Ratio". *IEEE Transactions on Magnetics*, 54(11), pp.1-4.

HUMBERT G, ROOSENDAAL C, SWANEPOEL JK, NAVARRO H, LE ROUX WG, SCIACOVELLI A (2022) Development of a latent heat thermal energy storage unit for the exhaust of a recuperated solar-dish Brayton cycle.

Ibaraki, S., Yamashita, Y., Sumida, K., Ogita, H., Jinnai, Y. (2006) 'Development of electrically assisted turbocharger', Hybrid turbo,Mitsubishi Heavy Industries Technical Review Vol.46 No. 3

Keogh, R. (2015) '40 kW Turbo-Alternator Hybrid-Electric Range Extender', *AHS Transformative Vertical Flight Concepts Workshop*.

Le Roux, W. G. and Sciacovelli, A. (2019) 'Recuperated solar-dish Brayton cycle using turbocharger and short-term thermal storage', *Solar Energy*. Elsevier, 194(September), pp. 569–580. doi: 10.1016/j.solener.2019.10.081.

Lee, T.W. and Hong, D.K. (2021) "Electrical and mechanical characteristics of a high-speed motor for electric turbochargers in relation to eccentricity," *Energies*, 14(11). doi:10.3390/en14113340.

Lim, M.S., Kim, J.M., Hwang, Y.S., Hong, J.P. (2017) "Design of an Ultra-High-Speed Permanent-Magnet Motor for an Electric Turbocharger Considering Speed Response Characteristics," *IEEE/ASME Transactions on Mechatronics*, 22(2), pp. 774–784. doi:10.1109/TMECH.2016.2634160.

McDonald, C.F., Rodgers, C. (2002) The ubiquitous personal turbine – a power vision for the 21st century, J. Eng. Gas Turb. Power 124, 835–844.

Mills, D. (2004) "Advances in solar thermal electricity technology". *Solar Energy*, 76(1-3), pp.19-31.

MTT. (2022) *EnerTwin*. [online] Available at: <https://enertwin.com/enertwin/> [Accessed 13 March 2022].

Noguchi, T., Takata, Y*., Yamashita, Y., Komatsu, Y., Ibaraki, S.* (2007) "220,000-r/min, 2-kW PM motor drive for turbocharger," *Electrical Engineering in Japan (English translation of Denki Gakkai Ronbunshi)*, 161(3), pp. 31–40. doi:10.1002/eej.20408.

Ouedraogo, N. (2019) "Opportunities, Barriers and Issues with Renewable Energy Development in Africa: a Comprehensible Review". *Current Sustainable/Renewable Energy Reports*, 6(2), pp.52-60.

Pietsch, A., Brandes, D.J. (1989) “Advanced solar Brayton space power systems”, In: *Proceedings of the Intersociety Energy Conversion Engineering Conference (IECEC)*, Los Alamitos, CA (1989) 911–916.

R.K. Shah, Compact heat exchangers for micro-turbines, Retrieved: 11 June, 2017, Available at: https://www.cso.nato.int/pubs/rdp.asp?RDP=RTO-EN-AVT-131, (2005).

Ssebabi, B., Dinter, F., van der Spuy, J. and Schatz, M., 2019. Predicting the performance of a micro gas turbine under solar-hybrid operation. *Energy*, 177, pp.121-135.

Subramaniam, K. and Wan Saiful-Islam Wan Salim, (2021) “Modelling an Electrically Turbocharged Engine and Predicting the Performance Under Steady-State Engine”. *International Journal of Automotive and Mechanical Engineering*, 18(4).

Visser, W., Shakariyants, S. and Oostveen, M., (2011) “Development of a 3 kW Microturbine for CHP Applications”. *Journal of Engineering for Gas Turbines and Power*, 133(4).

W.G. Le Roux (2018) “Feasibility study of a hybrid small-scale dish-mounted solar thermal Brayton cycle with cogeneration”, China, IHTC, Beijing, pp. 7929–7936.

Xiao, G. *et al.* (2017) “Recuperators for micro gas turbines: A review,” *Applied Energy*. Elsevier Ltd, pp. 83–99. doi:10.1016/j.apenergy.2017.03.095.